

Relational Representation Learning Network for Cross-Spectral Image Patch Matching

Chuang Yu^{1,2}, Yunpeng Liu^{1*}, Jinmiao Zhao^{1,2}, Dou Quan³, and Zelin Shi¹

¹ Shenyang Institute of Automation, Chinese Academy of Sciences

² University of Chinese Academy of Sciences

³ Xidian University

{yuchuang, ypliu, zhaojinmiao, zlshi}@sia.cn, dquan@stu.xidian.edu.cn

Abstract. Recently, feature relation learning has drawn widespread attention in cross-spectral image patch matching. However, existing related research focuses on extracting diverse relations between image patch features and ignores sufficient intrinsic feature representations of individual image patches. Therefore, an innovative relational representation learning idea is proposed for the first time, which simultaneously focuses on sufficiently mining the intrinsic features of individual image patches and the relations between image patch features. Based on this, we construct a lightweight **Relational Representation Learning Network** (RRL-Net). Specifically, we innovatively construct an autoencoder to fully characterize the individual intrinsic features, and introduce a Feature Interaction Learning (FIL) module to extract deep-level feature relations. To further fully mine individual intrinsic features, a lightweight Multi-dimensional Global-to-Local Attention (MGLA) module is constructed to enhance the global feature extraction of individual image patches and capture local dependencies within global features. By combining the MGLA module, we further explore the feature extraction network and construct an Attention-based Lightweight Feature Extraction (ALFE) network. In addition, we propose a Multi-Loss Post-Pruning (MLPP) optimization strategy, which greatly promotes network optimization while avoiding increases in parameters and inference time. Extensive experiments demonstrate that our RRL-Net achieves state-of-the-art (SOTA) performance on multiple public datasets. *Our code will be made public later.*

Keywords: Cross-spectral image patch matching · Image intrinsic features · Relational representation learning

1 Introduction

Image patch matching is to determine whether image patches come from the same interest point or have the same identity. It is widely used in image registration [38, 41, 59], image retrieval [14, 49], re-identification [56, 63] and other fields [45, 46, 65]. Different from other tasks that require the precise location of object boundaries [19, 35, 61], image patch matching focuses on measuring the similarity between image patches [40, 68]. Considering that single-spectral images have limitations, cross-spectral image matching can establish the correspondence

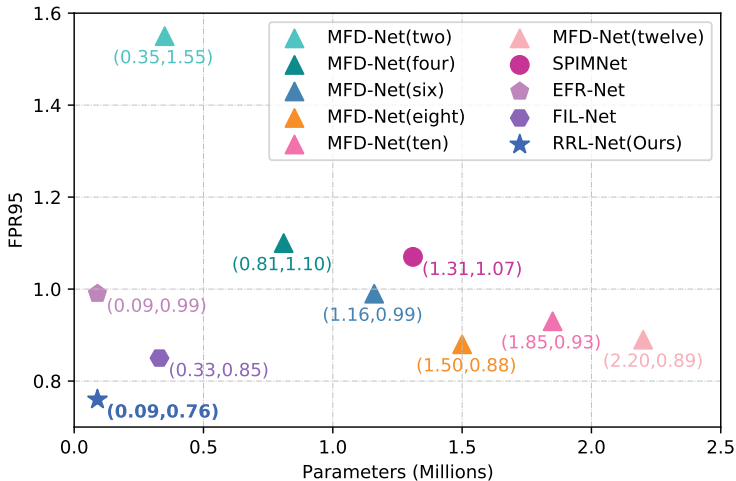


Fig. 1: Performance comparison of multiple excellent cross-spectral image patch matching networks on the VIS-NIR patch dataset. The content in the brackets of MFD-Net denotes the number of network branches. Our RRL-Net achieves SOTA performance. Compared with the lightweight EFR-Net [69], RRL-Net has the same parameters and reduces FPR95 by **23.2%** (from 0.99 to 0.76). Compared with the latest and most competitive FIL-Net [68], RRL-Net reduces FPR95 by **10.6%** (from 0.85 to 0.76) and reduces parameters by **72.7%** (from 0.33 to 0.09).

between different spectral images, providing a basis for making full use of the complementary information [1, 33, 37, 39, 67]. Of course, compared with single-spectral image patch matching, cross-spectral image patch matching not only faces illumination changes and geometric changes, but also needs to overcome pixel-level nonlinear differences between cross-spectral image patches [68, 69].

Early deep learning-based cross-spectral image patch matching methods use individual image patch features for discrimination [1, 2, 15]. Considering that this task is to measure the similarity between image patches, the relation learning between image patch features is better than the learning of individual image patch features [29, 40, 68]. Therefore, subsequent deep learning-based methods [25, 36, 37, 39, 67–69] focus on extracting diverse feature relations. However, sufficient representation of the individual intrinsic features is the basis for subsequent mining of feature relations. Only focusing on the diverse feature relations will limit the improvement of matching performance.

To solve this problem, an innovative relational representation learning idea is proposed for the first time, which simultaneously focuses on fully mining the intrinsic features of individual image patches and the relations between image patch features. This idea breaks the bottleneck of subsequent feature relation extraction caused by insufficient intrinsic feature mining of individual image patches in existing methods, and provides a new exploration direction for subsequent research on methods based on feature relation learning. Based on this idea, we explore the use of self-supervised learning to emphasize the mining of individual intrinsic features and innovatively construct an autoencoder. At the same time, a feature interaction learning (FIL) module [68] is introduced to interactively learn the intrinsic features of image patches to mine rich and deep-level feature relations.

Considering the small size of image patches and the goal of the matching task is to explore overall similarity rather than strong correspondence between pixels, we consider that in addition to the local features of image patches, global features should be given more attention. Therefore, we propose a Multi-dimensional Global-to-Local Attention (MGLA) module, which can extract global features from multiple dimensions and mine local dependencies within global features. The parameters of the MGLA module are negligible. In addition, combined with the MGLA module, we further explore the feature extraction network (encoder). An Attention-based Lightweight Feature Extraction (ALFE) network is constructed, which not only has powerful feature extraction capabilities but also has few parameters.

Considering that reasonably strong supervision can promote matching network optimization, we propose a Multi-Loss Post-Pruning (MLPP) optimization strategy, which not only has the advantage of promoting network optimization by adding feature reconstruction branches and multiple metric networks, but also avoids the disadvantages of increased parameters and reduced inference speed.

In summary, we propose a lightweight Relational Representation Learning Network (RRL-Net) to fully characterize the effective feature relations between image patches. From Fig. 1, our RRL-Net has achieved significant performance improvements in both matching results and parameters. In addition, we have also achieved SOTA results on multiple other cross-spectral datasets and conducted detailed ablation experiments to verify the effectiveness of each proposed component. Our contributions can be summarized as follows:

- An innovative relational representation learning idea is proposed, which breaks the bottleneck of subsequent feature relation extraction caused by insufficient individual intrinsic feature mining in existing methods.
- We innovatively construct an autoencoder that uses self-supervised learning to fully characterize the individual intrinsic features. At the same time, we introduce a FIL module to mine the deep-level feature relations.
- To further fully mine individual intrinsic features, a lightweight MGLA module is proposed and an efficient ALFE network is built based on this module.
- A MLPP optimization strategy is proposed that can promote network optimization while avoiding the increase in parameters and inference time.

2 Related Work

In this section, we provide a brief overview of previous research on single-spectral image patch matching methods, cross-spectral image patch matching methods, and attention mechanisms.

Single-spectral Image Patch Matching. Early single-spectral image patch matching methods are mainly non-deep learning methods [4, 5, 8, 9, 12, 24, 27, 29, 42, 43, 53, 54]. With the development of artificial intelligence, deep learning-based methods have gradually become a trend. Deep learning-based methods can be divided into descriptor learning methods and metric learning methods. The descriptor learning method extracts high-level features (descriptors) of individual

image patches and uses feature distance to measure the similarity between descriptors. It focuses on the improvement of loss functions [6, 7, 26, 31, 47, 50, 52, 58, 66, 72] and sampling strategies [30, 51, 55, 74]. Different from the descriptor learning method, the metric learning method is an end-to-end deep learning network, which focuses on improving the network structure [18, 40, 70].

Cross-spectral Image Patch Matching. Early cross-spectral image patch matching methods [1, 3, 16, 32, 34] are inspired by single-spectral image matching methods. Subsequently, the SCFDM [36] proposes extracting semantically invariant features between cross-spectral image patches in a shared semantic feature space, which reveals that the exploration of relations between cross-spectral image patch features will be superior to the feature extraction of image patches. Therefore, multiple methods [25, 37, 39, 67, 69] based on feature relation learning have been proposed, such as AFD-Net [37, 39], MFD-Net [67], and EFR-Net [69]. However, they can only extract shallow feature relations by directly using operations such as feature difference learning. Therefore, [68] proposes a feature interaction learning idea and constructs the FIL-Net, which can extract richer and deeper feature relations. However, the above methods based on feature relation learning focus on extracting diverse relations between image patch features and ignore the full representation of the individual image patch intrinsic features. Sufficient representation of the individual intrinsic features is the basis for subsequent mining of feature relations. Therefore, we attempt to explore sufficient representation learning of the individual intrinsic features and the feature relations.

Attention Mechanisms. Vision-based attention mechanisms can be roughly divided into channel attention, spatial attention and self-attention. Channel attention considers the importance of each channel [20, 57, 69, 71], such as the SE module [20] and ECA module [57]. Similar to channel attention, spatial attention aims to capture the importance of different regions in the spatial dimension [22, 28, 62, 73], such as the CBAM module [62]. Self-attention obtains larger receptive fields and contextual information by capturing global information [11, 17, 21, 60], such as Non-local block [60] and GC block [11]. Although the above attention modules have achieved great performance in corresponding tasks, there are few existing attention modules for cross-spectral image patch matching. Therefore, combined with the characteristics of the task, we attempt to build an efficient attention module to effectively extract the global features of image patches and the local dependencies within the global features.

3 Method

3.1 Overall Architecture

To efficiently extract discriminative features between cross-spectral image patches, we propose a lightweight RRL-Net to fully characterize the feature relations between them. Fig. 2 shows the overall architecture of RRL-Net, which adopts a modular design. It consists of five parts: feature extraction (encoder), feature reconstruction (decoder), feature interaction, feature aggregation and feature

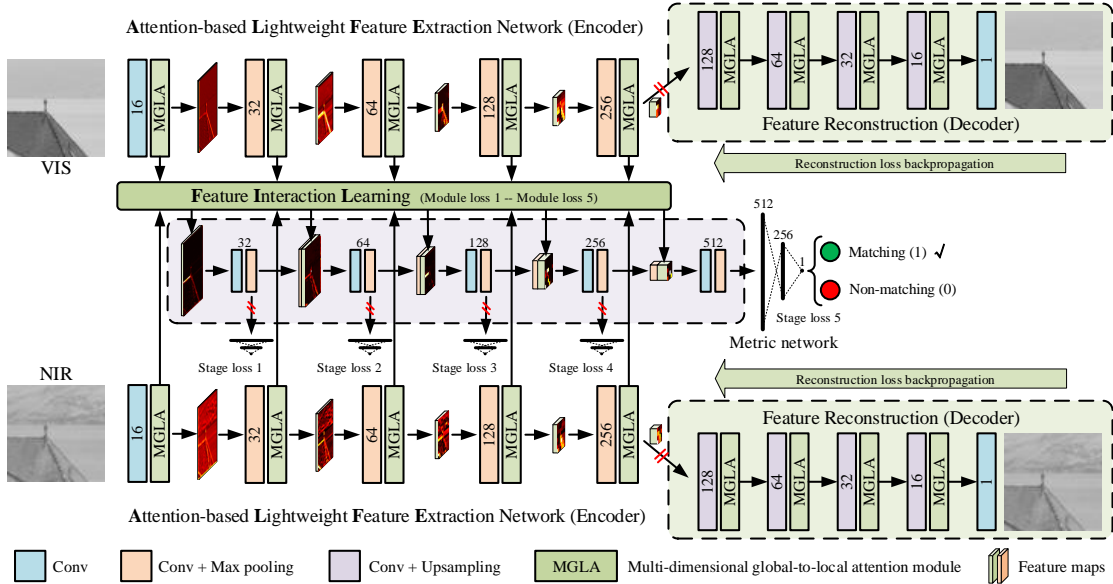


Fig. 2: Network structure of RRL-Net. The red slash denotes post-pruning operation.

metric. In the feature extraction part, we build a lightweight MGLA module that can fully extract global features from multiple dimensions and mine local dependencies within global features. In addition, combined with the MGLA module, an efficient ALFE network for cross-spectral image patches is constructed and used. In the feature reconstruction part, we build a feature reconstruction branch, which forms an autoencoder with the ALFE network. The feature reconstruction branch will drive the ALFE network to fully mine individual intrinsic features through self-supervised learning. It is conducive to the subsequent extraction of rich feature relations. For the feature interaction part, we introduce the FIL module, which is proposed in [68]. It can effectively consider common features and private features between image patch features. More details on this module can be found in the Supplementary Materials. For the feature aggregation part, its detailed structure is shown in the purple image area. We aggregate the private features output by the FIL module and learn again to improve feature discriminability. For the feature metric part, it contains all metric networks. Specifically, we perform a global average pooling on the feature map to convert it into a one-dimensional (1D) vector and measure the similarity through a 3-layer fully connected network, containing 512, 256 and 1 neurons respectively. Notably, except for the final metric network, which is used to output the similarity, other metric network branches and feature reconstruction branches will be pruned before the network model is saved.

3.2 Relational Representation Learning

The goal of cross-spectral image patch matching is to measure the similarity between image patches. The relation learning between image patch features is better than the learning of individual image patch features [40, 68, 69]. Existing methods based on feature relation learning focus on extracting diverse feature relations and ignore the full representation of the individual intrinsic features.

However, sufficient representation of the individual intrinsic features is the basis for subsequent mining of feature relations. Therefore, relational representation learning focuses on fully mining two aspects: the intrinsic features of individual image patches and the relations between image patch features.

To fully mine the intrinsic features of individual image patches, on the one hand, we conduct an in-depth exploration of the feature extraction network and propose an ALFE network, which has efficient image patch feature extraction capabilities and outputs five-stage feature maps. On the other hand, we reconstruct the high-level feature maps generated by the ALFE network using a feature reconstruction network (decoder). By constructing the autoencoder and using self-supervised learning, it is ensured that the ALFE network as the encoder can more fully characterize the intrinsic features of individual image patches.

To fully explore the relations between image patch features, we introduce the FIL module, which can effectively mine deep-level feature relations between cross-spectral image patches. This module fully explores the common and private features between image patches by strengthening the feature interaction, and promotes more discriminative private feature output by imposing reasonable constraints on the common features. To fully explore the multi-scale feature relations between image patches, we use five FIL modules on the corresponding feature maps of each stage output by the ALFE network and output five-stage multi-scale private features. At the same time, to extract multi-scale discriminative features, we use feature aggregation operations to sequentially aggregate multi-stage private features.

3.3 MGLA Module

For an image patch with a size of only 64×64 pixels, the effective local features that can be extracted are limited. Convolution is local perception. A feature extraction network constructed by simple stacked convolution will extract a large number of invalid or repeated local features. At the same time, unlike tasks such as object segmentation, which require precise positioning of object boundaries, matching tasks focus on whether images match. Fully considering the global features of image patches will be more helpful in extracting richer effective features. Therefore, we propose a MGLA module and reasonably embed it into the network.

From Fig. 3, the proposed MGLA module performs the same operation from three different dimensions H , W and C . Below, we take the channel dimension C as an example to illustrate. We first extract the global context through the attention pooling operation and output a 1D global feature vector. This operation does not contain any learning parameters and is formulated as:

$$G_c^i = DT(Re(F^i)) \otimes Softmax(Re(GAP_c(F^i))) \quad (1)$$

where GAP_c denotes global average pooling along the channel dimension. Re denotes the *Reshape* operation. DT denotes dimension transformation.

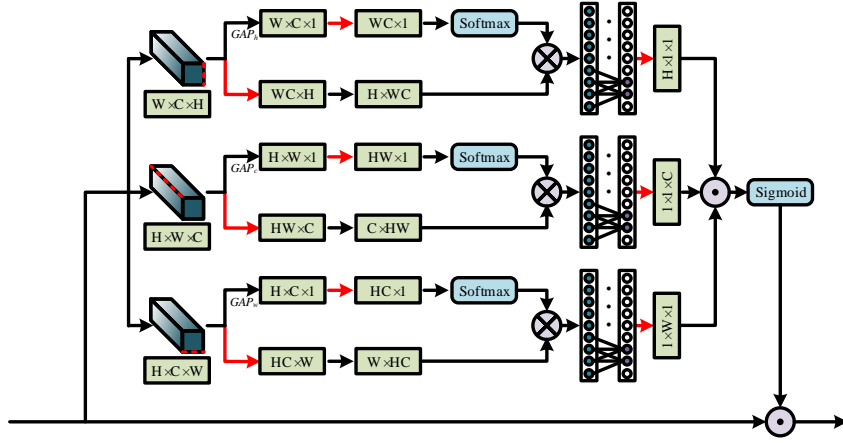


Fig. 3: Structure of the MGLA module. GAP denotes the global average pooling. \otimes denotes the matrix multiplication. \odot denotes the element-wise multiplication. The red arrow denotes the *Reshape* operation.

Then, to further capture the dependencies between channels [11, 60] and consider the impact of SENet compressed channels on performance improvement [57], we perform local interactions within global features:

$$GL_c^i = \varphi_c^i(G_c^i) \quad (2)$$

where φ_c^i denotes the 1D convolution operation on channel dimension C in the i_{th} MGLA module.

The convolution kernel size is determined based on the 1D vector length, formulated as:

$$k = \left\lceil \frac{\log_2^{len(G_c^i)} + 1}{2} \right\rceil \quad (3)$$

$$k = \begin{cases} k & k \% 2 = 0 \\ k + 1 & k \% 2 \neq 0 \end{cases} \quad (4)$$

where $len(G_c^i)$ denotes the 1D global context vector length of the i_{th} stage. $\lceil \cdot \rceil$ denotes rounding up. k denotes the 1D convolution kernel size. $\%$ denotes the remainder operation.

Each pixel in the image generally has a stronger correlation with its surrounding pixels. To extract richer global effective features and local dependencies within global features, our operation on the channel dimension is extended to spatial dimensions and pays attention to the effective features of the original feature map:

$$F_{out}^i = F^i \odot (Sigmoid(Re(GL_h^i) \odot Re(GL_w^i) \odot Re(GL_c^i))) \quad (5)$$

where GL_h^i and GL_w^i denote the outputs of spatial dimensions H and W .

In addition, combined with the MGLA module, we conduct an in-depth exploration of the feature extraction network for cross-spectral image patches. We find that the MGLA module can promote the reduction of stacked convolutions and cross-layer connections at each stage, thereby turning the constructed ALFE network into a lightweight and effective feature extraction network. The details of the experiments are provided in Sec. 4.5.

3.4 MLPP Optimization Strategy

We propose a MLPP optimization strategy that can greatly improve matching performance. The overall loss consists of two parts: reconstruction loss and metric loss. It can be formulated as follows:

$$L_{all} = L_m + \alpha \sum_{j=1}^2 L_r^j \quad (6)$$

where L_{all} , L_m , and L_r^j denote the total loss, metric loss, and reconstruction loss, respectively. α is set to 1. Its detailed experiments can be found in the Supplementary Materials.

To fully mine the intrinsic features of individual image patches, we constrain the reconstructed image by a combination of perceptual loss [23] and MSE loss. The reconstruction loss is formulated as:

$$L_r^j = \sqrt{(\varphi_p(P_r^j) - \varphi_p(P^j))^2} + \beta \left(\sqrt{(P_r^j - P^j)^2} \right) \quad (7)$$

where P_r^j and P^j denote the reconstructed image and original image, respectively. φ_p denotes a VGG19 network [48] pretrained on ImageNet [13]. β is set to 0.1.

To fully mine the relations between image patch features, we use multiple metric networks to impose strong constraints on the extracted relation features. Similar to [68], on the one hand, we use a metric network in the FIL module to constrain the extracted common features, which is called module loss. On the other hand, we use a metric network on the aggregated private features output at each stage, which is called stage loss. The metric loss is formulated as:

$$L_m(\hat{y}^i, \hat{y}^j, y) = \sum_{i=a}^5 L_{module}(\hat{y}^i, y) + \sum_{j=b}^5 L_{stage}(\hat{y}^j, y) \quad (8)$$

$$L(\hat{y}, y) = -[y \log(\hat{y}) + (1 - y) \log(1 - \hat{y})] \quad (9)$$

where L_{module} and L_{stage} denote module loss and stage loss, respectively. \hat{y}^i and \hat{y}^j are the actual outputs of the FIL modules and aggregated features through the metric network. y denotes the true label. We call the metric network used to output the final similarity the master metric network. Other metric networks are called sub-metric networks. Considering that excessive constraints on low-level feature maps using sub-metric branches will cause them to focus too much on semantic features and neglect to extract detailed features that should be provided to the main network, we appropriately reduce the strong constraints on low-level feature maps. The experiments in Sec. 4.5 verify that both a and b should be set to 3.

If the multi-loss strategy is used directly, it will bloat the final model and affect the inference speed. Therefore, we propose a post-pruning strategy. Specifically, before saving the generated model, we prune all branches that do not interfere with the normal output during the inference phase. By using post-pruning, the parameters of the final saved model will be greatly reduced, and the inference speed will be greatly improved.

4 Experiments

4.1 Dataset

We conduct experiments on four different cross-spectral datasets: VIS-NIR patch dataset [1, 10], OS patch dataset [64, 69], SEN1-2 patch dataset [44, 68] and VIS-NIR registration dataset. The VIS-NIR patch dataset is a visible spectrum (VIS) and near-infrared (NIR) image patch matching dataset. It contains more than 1.6 million image patch pairs, which are divided into 9 subsets. The experiment is trained on the “Country” subset and tested on the other eight subsets. The OS patch dataset and SEN1-2 patch dataset are both VIS and SAR image patch matching datasets. The former contains 123,676 samples. The latter contains 800,000 samples. The VIS-NIR registration dataset is a VIS and NIR registration dataset that we construct based on the VIS-NIR scene dataset [10]. Consistent with the experiments on the VIS-NIR patch dataset, the “Country” subset is used for training and the other eight subsets are used for testing. More details can be found in the Supplementary Materials.

4.2 Implementation Details

The epochs, learning rate, and batch size are set to 40, $2e-4$, and 64, respectively. To avoid the network from falling into overfitting, data augmentation operations such as flipping, rotation, and contrast enhancement are used. For image patch matching, consistent with [1, 2, 15, 25, 36, 37, 39, 40, 67–69], FPR95 is used as the evaluation metric. For cross-spectral image registration, the *RMSE* and image registration rate I_{rr} are used as the evaluation metrics [38, 41, 68]. The image after affine transformation with *RMSE* less than 5 is called a registered image. A detailed introduction to the evaluation metrics can be found in the Supplementary Materials.

4.3 Quantitative Results

In this section, we conduct detailed quantitative comparisons with multiple recent SOTA methods on the four datasets mentioned in Sec. 4.1. In the results presented, bold denotes the optimal results and underline denotes the suboptimal results. If not specified, “MFD-Net” denotes the eight-branch MFD-Net. In addition to the results presented in this section, more quantitative results can be found in the Supplementary Materials.

Performance comparison on the VIS-NIR patch dataset. As shown in Tab. 1. From the individual results of the eight subsets, our RRL-Net has excellent generalizability. From the mean results of eight subsets, RRL-Net achieves SOTA results. Compared with the latest FIL-Net, RRL-Net reduces the FPR95 by 10.6% (from 0.85 to 0.76). Notably, compared to MFD-Net in 2022, FIL-Net, which has the best results in 2023, only reduces by 3.4% (from 0.88 to 0.85). In addition, according to the statistics, the parameters of RRL-Net only account for 27.3% of it, and the inference speed of RRL-Net is 1.78 times that of it.

Table 1: Performance comparison on the VIS-NIR patch dataset.

Models	Field	Forest	Indoor	Mountain	Oldbuilding	Street	Urban	Water	Mean
Traditional methods									
SIFT [29][IJCV'04]	39.44	11.39	10.13	28.63	19.69	31.14	10.85	40.33	23.95
GISIFT [16][ICIP'11]	34.75	16.63	10.63	19.52	12.54	21.80	7.21	25.78	18.60
LGHD [3][ICIP'15]	16.52	3.78	7.91	10.66	7.91	6.55	7.21	12.76	9.16
Descriptor learning									
Q-Net [2][Sensors'17]	17.01	2.70	6.16	9.61	4.61	3.99	2.83	8.44	6.91
L2-Net [51][CVPR'17]	13.67	2.48	4.63	8.87	4.12	5.58	1.54	6.55	5.93
HardNet [30][NeurIPS'17]	5.61	0.15	1.50	3.14	1.10	1.93	0.69	2.29	2.05
SOSNet [52][CVPR'19]	5.94	0.13	1.53	2.45	0.99	2.04	0.78	1.90	1.97
HyNet [50][NeurIPS'20]	4.50	0.07	1.09	1.80	0.83	0.52	0.53	1.91	1.41
Metric learning									
Siamese [1][CVPRW'16]	15.79	10.76	11.60	11.15	5.27	7.51	4.60	10.21	9.61
Pseudo-Siamese [1][CVPRW'16]	17.01	9.82	11.17	11.86	6.75	8.25	5.65	12.04	10.31
2-channel [1][CVPRW'16]	9.96	0.12	4.40	8.89	2.30	2.18	1.58	6.40	4.47
SCFDM [36][ACCV'18]	7.91	0.87	3.93	5.07	2.27	2.22	0.85	4.75	3.48
MR_3A [40][TIP'21]	4.21	0.11	1.12	0.87	0.67	0.56	0.43	1.90	1.23
AFD-Net [37,39][ICCV'19,TNNLS'21]	3.47	0.08	1.48	<u>0.68</u>	0.71	0.42	0.29	<u>1.48</u>	1.08
SPIMNet [25][Inf. Fusion'23]	<u>2.28</u>	0.09	1.62	0.88	0.69	0.29	0.42	2.26	1.07
EFR-Net [69][TGRS'23]	2.84	0.07	1.09	0.79	0.61	0.50	0.34	1.65	0.99
MFD-Net [67][TGRS'22]	2.59	0.02	1.24	0.95	<u>0.48</u>	0.24	<u>0.12</u>	1.44	0.88
FIL-Net [68][TIP'23]	2.61	<u>0.04</u>	<u>0.98</u>	0.73	0.49	0.34	0.10	1.49	<u>0.85</u>
RRL-Net (Ours)	2.16	<u>0.04</u>	0.86	0.59	0.41	<u>0.26</u>	0.14	1.65	0.76

Performance comparison on the OS patch dataset. As shown in Fig. 4a. Our RRL-Net achieves SOTA results on the OS patch dataset. Compared with AFD-Net, MFD-Net(eight), EFR-Net and FIL-Net, RRL-Net reduced FPR95 by 31.5% (from 7.62 to 5.22), 21.9% (from 6.68 to 5.22), 13.4% (from 6.03 to 5.22) and 2.8% (from 5.37 to 5.22), respectively.

Performance comparison on the SEN1-2 patch dataset. Combining the results in Fig. 4a and Fig. 4b, the FPR95 of AFD-Net, MFD-Net, FIL-Net and RRL-Net is significantly different between the two datasets, and the FPR95 of EFR-Net and MR_3A is not much different between the two datasets. In addition, they achieve better results on the SEN1-2 patch dataset. This is because the SEN1-2 patch dataset has more samples, while the OS patch dataset has more semantic scenes, such as houses and airplanes. Meanwhile, EFR-Net and MR_3A only use the highest-level feature maps and focus on semantic features. In addition, our RRL-Net achieves SOTA results on the SEN1-2 patch dataset. Compared with the latest FIL-Net, RRL-Net reduced the mean FPR95 by 10.9% (from 1.56 to 1.39).

Performance comparison on VIS-NIR registration dataset. We apply our RRL-Net to the cross-spectral image registration task. Different from taking the first 5 samples of eight subsets in [68], we take the first 20 samples to form 160 samples to better evaluate the method performance. From Tab. 2, our RRL-Net achieves the best results in $mRMSE$ and suboptimal results in registration rate, which shows that our RRL-Net has excellent robustness in cross-spectral image registration. In addition, RRL-Net has the most registered samples with

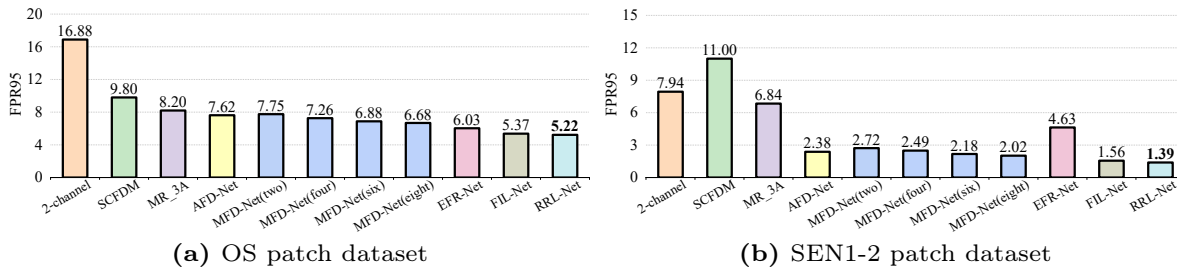


Fig. 4: Performance comparison on two VIS-SAR image patches datasets

Table 2: Registration results on the VIS-NIR registration dataset.

Methods	RMSE distribution			$I_{rr} \uparrow$	$mRMSE \downarrow$
	$<1 \uparrow$	$1\sim5$	$>5 \downarrow$		
SCFDM [36]	121	29	10	93.8%	8.48
AFD-Net [37, 39]	121	29	10	93.8%	9.30
MR_3A [40]	118	31	11	93.1%	10.43
MFD-Net [67]	125	30	5	96.9%	5.57
EFR-Ne [69]	124	30	6	96.3%	4.95
FIL-Net [68]	115	38	7	95.6%	5.27
RRL-Net (Ours)	127	27	6	96.3%	4.62

RMSE less than 1. This shows that RRL-Net has a more refined cross-spectral image registration effect.

4.4 Qualitative Results

To intuitively demonstrate the matching effects in multiple cross-spectral scenarios, we conduct a qualitative analysis of the proposed RRL-Net in this section. In addition to the results presented in this section, more quantitative results can be found in the Supplementary Materials.

VIS-NIR image patch matching. As shown in Fig. 5. From the samples misjudged as non-matching, most individual samples in pairs have unclear features. At the same time, due to the movement of objects, there are samples that are marked as matching but visually non-matching. From the samples misjudged as matching, most samples have obviously similar semantic features. From the samples that are correctly judged as non-matching, RRL-Net can correctly distinguish non-matching samples with partially similar semantic features. From the samples that are correctly judged as matching, there are obvious nonlinear differences between cross-spectral image patches. This proves that RRL-Net is robust for VIS-NIR scenarios.

VIS-SAR image patch matching. As shown in Fig. 6. From the samples misjudged as non-matching, there is a common problem of feature scarcity in SAR images. For texture or semantic features in VIS images, there are no obvious corresponding features in SAR images. From the samples misjudged as matching, there are similar semantic features in VIS and SAR images. From the samples that are correctly judged, RRL-Net can also correctly identify non-matching samples with partially similar semantic features and matching samples with pixel-level nonlinear differences. This proves that RRL-Net is robust for VIS-SAR scenarios.

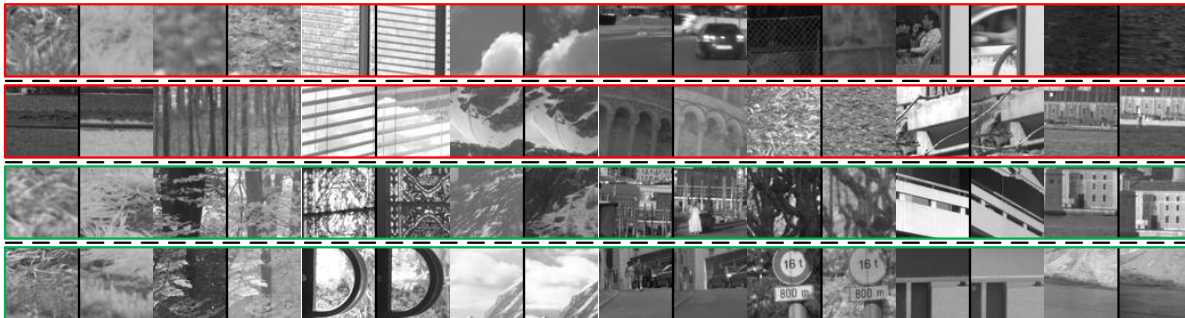


Fig. 5: Partial matching results of RRL-Net on the VIS-NIR patch dataset. From top to bottom, the four lines of samples are misjudged as non-matching, misjudged as matching, correctly judged as non-matching, and correctly judged as matching.

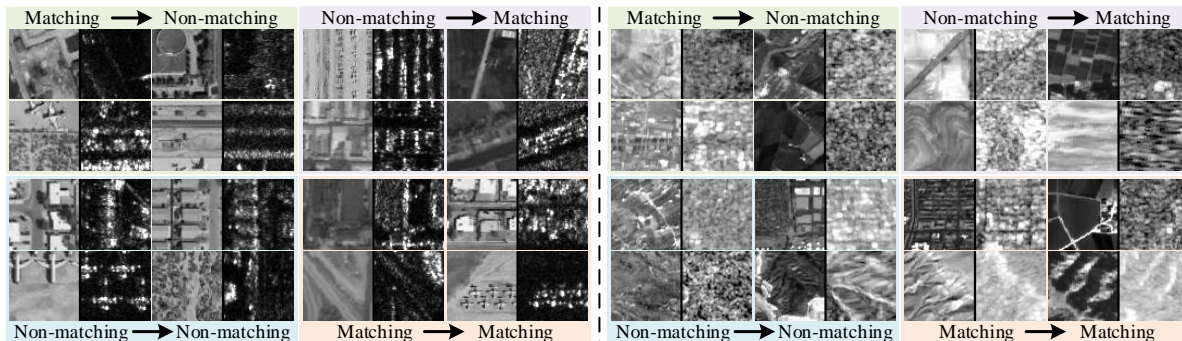


Fig. 6: Partial results of RRL-Net on two VIS-SAR datasets. The left and right samples are from the OS patch dataset and SEN1-2 patch dataset respectively. The left and right sides of the arrow denote the true labels and predicted results, respectively.

4.5 Ablation Study

This section conducts extensive ablation experiments to study the effects of each component in our proposed method. In the results presented, values in parentheses indicate differences from the final results.

Break-down Ablation. We first explore the influence of each component in RRL-Net on matching performance. From Tab. 3a, the MGLA module, FIL module and MLPP optimization strategy can reduce the FPR95 by 33.3%, 25.5% and 24.8%, respectively. These results verify the significant effectiveness of each component.

MGLA Module. From Tab. 3c, **firstly**, adding an attention module can improve the matching results, and our MGLA module achieves SOTA results with negligible parameter increase. **Secondly**, from the results of SE, ECA, ELA and MGLA, not using dimensionality reduction but enhancing local interactions within global features will help improve the matching performance. **Thirdly**, from the results of SE and CBAM, simply adding a spatial attention branch to focus on local spatial features will worsen the matching results. At the same time, combining the results of SNL, GC and MGLA, paying more attention to global features will significantly improve the matching results. **Finally**, the improvement effect of adding the CGLA module is significantly better than that of HGLA and WGLA. This shows that compared with paying attention

Methods	Variants			FPR95↓	Attention modules	FPR95 ↓	Parameters ↓	
	MGLA	FIL	MLPP					
Our-w/o MGLA	✗	✓	✓	1.14 (-33.3%)	Our-w/o MGLA	1.14 (-33.3%)	9,403,905 (+120)	
Our-w/o FIL	✓	✗	✓	1.02 (-25.5%)	SE (r=4) ^[20]	0.93 (-18.3%)	9,492,441 (-0.9%)	
Our-w/o MLPP	✓	✓	✗	1.01 (-24.8%)	SE (r=8) ^[20]	0.98 (-22.4%)	9,448,669 (-0.5%)	
RRL-Net (Ours)	✓	✓	✓	0.76	SE (r=16) ^[20]	1.07 (-29.0%)	9,426,783 (-0.2%)	
(a) Break-down ablation								
Methods	CL		CC	FPR95 ↓	Parameters↓	Attention modules		
	1	2 3				1 2 3	1 2 3	
Variant 1	✗	✗	✓	0.83 (-8.4%)	12,648,441 (-25.7%)	ECA ^[57]	0.83 (-8.4%)	9,403,953 (+72)
Variant 2	✗	✗	✗	0.91 (-16.5%)	12,556,601 (-25.1%)	ELA ^[69]	0.81 (-6.2%)	9,404,025
Variant 3	✗	✓	✓	0.80 (-5.0%)	11,072,153 (-15.1%)	CBAM (r=4) ^[62]	0.97 (-21.6%)	9,493,421 (-0.9%)
Variant 4	✗	✓	✗	0.84 (-9.5%)	10,980,313 (-14.4%)	SNL ^[11]	0.94 (-19.1%)	9,580,491 (-1.8%)
Variant 5	✓	✗	✓	0.82 (-7.3%)	9,495,865 (-1.0%)	GC (r=4) ^[11]	0.90 (-15.6%)	9,494,435 (-1.0%)
ALFE (Ours)	✓	✗	✗	0.76	9,404,025	HGLA (Ours)	1.08 (-29.6%)	9,403,941 (+84)
						WGLA (Ours)	1.05 (-27.6%)	9,403,941 (+84)
						CGLA (Ours)	0.79 (-3.8%)	9,403,953 (+72)
						MGLA (Ours)	0.76	9,404,025

(b) Exploration of ALFE network

(c) Exploration of MGLA module

Table 3: Ablation experiments on VIS-NIR patch dataset. CL: Convolutional layers before each MGLA module, CC: Cross-layer connection. r is compression ratio. HGLA, WGLA, and CGLA are single dimension H , W , and C global-to-local attention.

to other dimensions, fully considering the global context and strengthening the local interaction within the global context have more obvious improvements. Of course, the MGLA module results show that extracting multi-dimensional features has better results.

ALFE network. Consistent with the exploration of [68], we explore the number of convolutional layers (before each MGLA module) and cross-layer connections at each stage. [68] achieves the optimal matching result by using 3 convolutional layers and applying cross-layer connections. However, from Tab. 3b, when using our MGLA module, the optimal number of convolutional layers is 1, and no cross-layer connections are used. Compared with Variant 1-Variant 5, the FPR95 and parameters of the ALFE network are reduced by 5.0% - 16.5% and 1.0% - 25.7%.

MLPP optimization strategy. We conduct an in-depth exploration. From Fig. 7, when the added module loss and stage loss are both 3, RRL-Net has the lowest FPR95, which verifies that the reasonable addition of multiple metric branches can effectively improve network performance. From Tab. 4, compared with not using the MLPP strategy, the reasonable addition of sub-metric networks and reconstruction branches will improve the matching results. At the same time, the improvement is more obvious when they are used superimposed, which can reduce the FPR95 by 24.8%. Of course, it will bring about an increase in network parameters and inference time. To solve this problem, we use post-pruning. Compared with simply using the multi-loss strategy, the MLPP optimization strategy has the same matching effect improvement, and its network parameters and single sample inference time are reduced by 26.7% and 25.9%, respectively. It is worth mentioning that compared with only adding sub-metric networks (Variant 2), which has achieved an excellent result of 0.83 in FPR95, adding additional reconstruction branches (Variant 5) will reduce FPR95 by 8.4% (from 0.83 to 0.76). This proves that fully mining individual intrinsic

Table 4: Ablation experiments of MLPP optimization strategy on VIS-NIR patch dataset. SN: Sub-metric network, RB: Reconstruction branches, RB-Loss: Reconstruction branch loss, ML: MSE loss, PL: Perceptual loss, PP: Post-pruning.

Methods	SN	RB	RB-Loss ML	PL	PP	FPR95 ↓	Parameters ↓	Inference time (s) ↓
Ours-w/o MLPP	✗	✗	✗	✗	✗	1.01 (-24.8%)	9,404,025	0.40×10^{-3}
Variant 1	✗	✓	✓	✓	✗	0.95 (-20.0%)	10,190,175 (-7.7%)	0.51×10^{-3} (-21.6%)
Variant 2	✓	✗	✗	✗	✗	0.83 (-8.4%)	12,043,262 (-21.9%)	0.44×10^{-3} (-9.1%)
Variant 3	✓	✓	✗	✓	✗	0.79 (-3.8%)	12,829,276 (-26.7%)	0.54×10^{-3} (-25.9%)
Variant 4	✓	✓	✓	✗	✗	0.79 (-3.8%)	12,829,276 (-26.7%)	0.54×10^{-3} (-25.9%)
Variant 5	✓	✓	✓	✓	✗	0.76	12,829,276 (-26.7%)	0.54×10^{-3} (-25.9%)
Ours-w/ MLPP	✓	✓	✓	✓	✓	0.76	9,404,025	0.40×10^{-3}

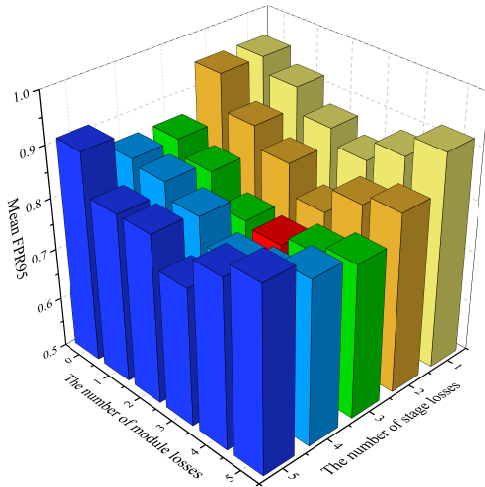


Fig. 7: The results of different combinations of stage loss and module loss on the VIS-NIR patch dataset. Losses are added from higher to lower levels. Red denotes the lowest value of 0.76.

features will help break the bottleneck of existing feature relation extraction, thereby achieving a significant improvement in matching performance.

5 Conclusion

In this work, we innovatively construct a lightweight RRL-Net, which breaks the bottleneck of subsequent feature relation extraction caused by insufficient intrinsic feature mining of individual image patches in existing methods. To solve the problem of insufficient extraction of individual intrinsic features, on the one hand, we propose a MGLA module and construct an ALFE network. On the other hand, we construct a feature reconstruction branch, which drives the ALFE network to fully characterize individual intrinsic features. For the relations between image patch features, we introduce a FIL module to fully mine the rich and deep-level feature relations. In addition, we construct a MLPP optimization strategy to promote network optimization. Extensive experimental results show that RRL-Net achieves significant performance improvements on multiple datasets.

References

1. Aguilera, C.A., Aguilera, F.J., Sappa, A.D., Aguilera, C., Toledo, R.: Learning cross-spectral similarity measures with deep convolutional neural networks. In: CVPRW. pp. 1–9 (2016) [2](#), [4](#), [9](#), [10](#)
2. Aguilera, C.A., Sappa, A.D., Aguilera, C., Toledo, R.: Cross-spectral local descriptors via quadruplet network. *Sensors* **17**(4), 873 (2017) [2](#), [9](#), [10](#)
3. Aguilera, C.A., Sappa, A.D., Toledo, R.: Lghd: A feature descriptor for matching across non-linear intensity variations. In: ICIP. pp. 178–181 (2015) [4](#), [10](#)
4. Alcantarilla, P.F., Bartoli, A., Davison, A.J.: Kaze features. In: ECCV. pp. 214–227 (2012) [3](#)
5. Alcantarilla, P., Nuevo, J., Bartoli, A.: Fast explicit diffusion for accelerated features in nonlinear scale spaces. In: BMVC (2013) [3](#)
6. Balntas, V., Johns, E., Tang, L., Mikolajczyk, K.: Pn-net: Conjoined triple deep network for learning local image descriptors. arXiv preprint arXiv:1601.05030 (2016) [4](#)
7. Balntas, V., Riba, E., Ponsa, D., Mikolajczyk, K.: Learning local feature descriptors with triplets and shallow convolutional neural networks. In: BMVC. vol. 1, p. 3 (2016) [4](#)
8. Barnea, D.I., Silverman, H.F.: A class of algorithms for fast digital image registration. *IEEE transactions on Computers* **100**(2), 179–186 (1972) [3](#)
9. Bay, H., Ess, A., Tuytelaars, T., Van Gool, L.: Speeded-up robust features (surf). *Computer vision and image understanding* **110**(3), 346–359 (2008) [3](#)
10. Brown, M., Süssstrunk, S.: Multi-spectral sift for scene category recognition. In: CVPR. pp. 177–184 (2011) [9](#)
11. Cao, Y., Xu, J., Lin, S., Wei, F., Hu, H.: Gcnet: Non-local networks meet squeeze-excitation networks and beyond. In: ICCVW. pp. 0–0 (2019) [4](#), [7](#), [13](#)
12. Dalal, N., Triggs, B.: Histograms of oriented gradients for human detection. In: CVPR. vol. 1, pp. 886–893 (2005) [3](#)
13. Deng, J., Dong, W., Socher, R., Li, L.J., Li, K., Fei-Fei, L.: Imagenet: A large-scale hierarchical image database. In: CVPR. pp. 248–255 (2009) [8](#)
14. Dou, Z., Wang, Z., Chen, W., Li, Y., Wang, S.: Reliability-aware prediction via uncertainty learning for person image retrieval. In: ECCV. pp. 588–605 (2022) [1](#)
15. En, S., Lechervy, A., Jurie, F.: Ts-net: Combining modality specific and common features for multimodal patch matching. In: ICIP. pp. 3024–3028 (2018) [2](#), [9](#)
16. Firmenichy, D., Brown, M., Süssstrunk, S.: Multispectral interest points for rgb-nir image registration. In: ICIP. pp. 181–184 (2011) [4](#), [10](#)
17. Fu, J., Liu, J., Tian, H., Li, Y., Bao, Y., Fang, Z., Lu, H.: Dual attention network for scene segmentation. In: CVPR. pp. 3146–3154 (2019) [4](#)
18. Han, X., Leung, T., Jia, Y., Sukthankar, R., Berg, A.C.: Matchnet: Unifying feature and metric learning for patch-based matching. In: CVPR. pp. 3279–3286 (2015) [4](#)
19. He, M., Wang, Y., Wu, J., Wang, Y., Li, H., Li, B., Gan, W., Wu, W., Qiao, Y.: Cross domain object detection by target-perceived dual branch distillation. In: CVPR. pp. 9570–9580 (2022) [1](#)
20. Hu, J., Shen, L., Albanie, S., Sun, G., Wu, E.: Squeeze-and-excitation networks. *IEEE transactions on pattern analysis and machine intelligence* **42**(8), 2011–2023 (2020) [4](#), [13](#)
21. Huang, Z., Wang, X., Huang, L., Huang, C., Wei, Y., Liu, W.: Ccnet: Criss-cross attention for semantic segmentation. In: CVPR. pp. 603–612 (2019) [4](#)

22. Jaderberg, M., Simonyan, K., Zisserman, A., et al.: Spatial transformer networks. *NeurIPS* **28** (2015) [4](#)
23. Johnson, J., Alahi, A., Fei-Fei, L.: Perceptual losses for real-time style transfer and super-resolution. In: *ECCV*. pp. 694–711 (2016) [8](#)
24. Ke, Y., Sukthankar, R.: Pca-sift: A more distinctive representation for local image descriptors. In: *CVPR*. vol. 2, pp. II–II (2004) [3](#)
25. Ko, Y., Jang, Y.J., Dinh, V.Q., Jeon, H.G., Jeon, M.: Spectral-invariant matching network. *Information Fusion* **91**, 623–632 (2023) [2](#), [4](#), [9](#), [10](#)
26. Kumar BG, V., Carneiro, G., Reid, I.: Learning local image descriptors with deep siamese and triplet convolutional networks by minimising global loss functions. In: *CVPR*. pp. 5385–5394 (2016) [4](#)
27. Leutenegger, S., Chli, M., Siegwart, R.Y.: Brisk: Binary robust invariant scalable keypoints. In: *ICCV*. pp. 2548–2555 (2011) [3](#)
28. Li, C., Du, D., Zhang, L., Wen, L., Luo, T., Wu, Y., Zhu, P.: Spatial attention pyramid network for unsupervised domain adaptation. In: *ECCV*. pp. 481–497 (2020) [4](#)
29. Lowe, D.G.: Distinctive image features from scale-invariant keypoints. *International journal of computer vision* **60**, 91–110 (2004) [2](#), [3](#), [10](#)
30. Mishchuk, A., Mishkin, D., Radenovic, F., Matas, J.: Working hard to know your neighbor’s margins: Local descriptor learning loss. *NeurIPS* **30** (2017) [4](#), [10](#)
31. Mishkin, D., Radenovic, F., Matas, J.: Repeatability is not enough: Learning affine regions via discriminability. In: *ECCV*. pp. 284–300 (2018) [4](#)
32. Mouats, T., Aouf, N., Sappa, A.D., Aguilera, C., Toledo, R.: Multispectral stereo odometry. *IEEE Transactions on Intelligent Transportation Systems* **16**(3), 1210–1224 (2014) [4](#)
33. Ofir, N., Silberstein, S., Levi, H., Rozenbaum, D., Keller, Y., Bar, S.D.: Deep multi-spectral registration using invariant descriptor learning. In: *ICIP*. pp. 1238–1242 (2018) [2](#)
34. Pinggera12, P., Breckon, T., Bischof, H.: On cross-spectral stereo matching using dense gradient features. In: *CVPR*. vol. 2, p. 3 (2012) [4](#)
35. Qin, X., Dai, H., Hu, X., Fan, D.P., Shao, L., Van Gool, L.: Highly accurate dichotomous image segmentation. In: *ECCV*. pp. 38–56 (2022) [1](#)
36. Quan, D., Fang, S., Liang, X., Wang, S., Jiao, L.: Cross-spectral image patch matching by learning features of the spatially connected patches in a shared space. In: *ACCV*. pp. 115–130 (2019) [2](#), [4](#), [9](#), [10](#), [11](#)
37. Quan, D., Liang, X., Wang, S., Wei, S., Li, Y., Huyan, N., Jiao, L.: Afd-net: Aggregated feature difference learning for cross-spectral image patch matching. In: *ICCV*. pp. 3017–3026 (2019) [2](#), [4](#), [9](#), [10](#), [11](#)
38. Quan, D., Wang, S., Gu, Y., Lei, R., Yang, B., Wei, S., Hou, B., Jiao, L.: Deep feature correlation learning for multi-modal remote sensing image registration. *IEEE Transactions on Geoscience and Remote Sensing* **60**, 1–16 (2022) [1](#), [9](#)
39. Quan, D., Wang, S., Huyan, N., Chanussot, J., Wang, R., Liang, X., Hou, B., Jiao, L.: Element-wise feature relation learning network for cross-spectral image patch matching. *IEEE Transactions on Neural Networks and Learning Systems* **33**(8), 3372–3386 (2021) [2](#), [4](#), [9](#), [10](#), [11](#)
40. Quan, D., Wang, S., Li, Y., Yang, B., Huyan, N., Chanussot, J., Hou, B., Jiao, L.: Multi-relation attention network for image patch matching. *IEEE Transactions on Image Processing* **30**, 7127–7142 (2021) [1](#), [2](#), [4](#), [5](#), [9](#), [10](#), [11](#)
41. Quan, D., Wei, H., Wang, S., Lei, R., Duan, B., Li, Y., Hou, B., Jiao, L.: Self-distillation feature learning network for optical and sar image registration. *IEEE Transactions on Geoscience and Remote Sensing* **60**, 1–18 (2022) [1](#), [9](#)

42. Rosenfeld, A.: Coarse-fine template matching. *IEEE Transaction on Systems Man and Cybernetics* **7**(2), 104–107 (1977) [3](#)
43. Rublee, E., Rabaud, V., Konolige, K., Bradski, G.: Orb: An efficient alternative to sift or surf. In: *ICCV*. pp. 2564–2571 (2011) [3](#)
44. Schmitt, M., Hughes, L.H., Qiu, C., Zhu, X.X.: Sen12ms—a curated dataset of georeferenced multi-spectral sentinel-1/2 imagery for deep learning and data fusion. *arXiv preprint arXiv:1906.07789* (2019) [9](#)
45. Seitz, S.M., Curless, B., Diebel, J., Scharstein, D., Szeliski, R.: A comparison and evaluation of multi-view stereo reconstruction algorithms. In: *CVPR*. vol. 1, pp. 519–528 (2006) [1](#)
46. Shi, Y., Xu, K., Nießner, M., Rusinkiewicz, S., Funkhouser, T.: Planematch: Patch coplanarity prediction for robust rgb-d reconstruction. In: *ECCV*. pp. 750–766 (2018) [1](#)
47. Simo-Serra, E., Trulls, E., Ferraz, L., Kokkinos, I., Fua, P., Moreno-Noguer, F.: Discriminative learning of deep convolutional feature point descriptors. In: *ICCV*. pp. 118–126 (2015) [4](#)
48. Simonyan, K., Zisserman, A.: Very deep convolutional networks for large-scale image recognition. In: *ICLR* (2015) [8](#)
49. Sun, B., Kim, V.G., Aigerman, N., Huang, Q., Chaudhuri, S.: Patchrd: detail-preserving shape completion by learning patch retrieval and deformation. In: *ECCV*. pp. 503–522 (2022) [1](#)
50. Tian, Y., Barroso Laguna, A., Ng, T., Balntas, V., Mikolajczyk, K.: Hynet: Learning local descriptor with hybrid similarity measure and triplet loss. *NeurIPS* **33**, 7401–7412 (2020) [4](#), [10](#)
51. Tian, Y., Fan, B., Wu, F.: L2-net: Deep learning of discriminative patch descriptor in euclidean space. In: *CVPR*. pp. 661–669 (2017) [4](#), [10](#)
52. Tian, Y., Yu, X., Fan, B., Wu, F., Heijnen, H., Balntas, V.: Sosnet: Second order similarity regularization for local descriptor learning. In: *CVPR*. pp. 11016–11025 (2019) [4](#), [10](#)
53. Vanderbrug, Rosenfeld: Two-stage template matching. *IEEE transactions on computers* **100**(4), 384–393 (1977) [3](#)
54. Viola, P., Wells III, W.: Alignment by maximization of mutual information. In: *ICCV*. pp. 16–16 (1995) [3](#)
55. Wang, C., Zhang, X., Lan, X.: How to train triplet networks with 100k identities? In: *ICCVW*. pp. 1907–1915 (2017) [4](#)
56. Wang, J., Zhang, Z., Chen, M., Zhang, Y., Wang, C., Sheng, B., Qu, Y., Xie, Y.: Optimal transport for label-efficient visible-infrared person re-identification. In: *ECCV*. pp. 93–109 (2022) [1](#)
57. Wang, Q., Wu, B., Zhu, P., Li, P., Zuo, W., Hu, Q.: Eca-net: Efficient channel attention for deep convolutional neural networks. In: *CVPR*. pp. 11534–11542 (2020) [4](#), [7](#), [13](#)
58. Wang, S., Li, Y., Liang, X., Quan, D., Yang, B., Wei, S., Jiao, L.: Better and faster: Exponential loss for image patch matching. In: *ICCV*. pp. 4812–4821 (2019) [4](#)
59. Wang, S., Quan, D., Liang, X., Ning, M., Guo, Y., Jiao, L.: A deep learning framework for remote sensing image registration. *ISPRS Journal of Photogrammetry and Remote Sensing* **145**, 148–164 (2018) [1](#)
60. Wang, X., Girshick, R., Gupta, A., He, K.: Non-local neural networks. In: *CVPR*. pp. 7794–7803 (2018) [4](#), [7](#)
61. Wang, X., Lin, J., Zhao, J., Yang, X., Yan, J.: Eautodet: Efficient architecture search for object detection. In: *ECCV*. pp. 668–684 (2022) [1](#)

62. Woo, S., Park, J., Lee, J.Y., Kweon, I.S.: Cbam: Convolutional block attention module. In: ECCV. pp. 3–19 (2018) [4](#), [13](#)
63. Wu, J., He, L., Liu, W., Yang, Y., Lei, Z., Mei, T., Li, S.Z.: Cavit: Contextual alignment vision transformer for video object re-identification. In: ECCV. pp. 549–566 (2022) [1](#)
64. Xiang, Y., Tao, R., Wang, F., You, H., Han, B.: Automatic registration of optical and sar images via improved phase congruency model. *IEEE Journal of Selected Topics in Applied Earth Observations and Remote Sensing* **13**, 5847–5861 (2020) [9](#)
65. Yan, X., Zhao, W., Yuan, K., Zhang, R., Li, Z., Cui, S.: Towards content-independent multi-reference super-resolution: Adaptive pattern matching and feature aggregation. In: ECCV. pp. 52–68 (2020) [1](#)
66. Yang, T.Y., Hsu, J.H., Lin, Y.Y., Chuang, Y.Y.: Deepcd: Learning deep complementary descriptors for patch representations. In: ICCV. pp. 3314–3322 (2017) [4](#)
67. Yu, C., Liu, Y., Li, C., Qi, L., Xia, X., Liu, T., Hu, Z.: Multibranch feature difference learning network for cross-spectral image patch matching. *IEEE Transactions on Geoscience and Remote Sensing* **60**, 1–15 (2022) [2](#), [4](#), [9](#), [10](#), [11](#)
68. Yu, C., Liu, Y., Zhao, J., Wu, S., Hu, Z.: Feature interaction learning network for cross-spectral image patch matching. *IEEE Transactions on Image Processing* (2023) [1](#), [2](#), [4](#), [5](#), [8](#), [9](#), [10](#), [11](#), [13](#)
69. Yu, C., Zhao, J., Liu, Y., Wu, S., Li, C.: Efficient feature relation learning network for cross-spectral image patch matching. *IEEE Transactions on Geoscience and Remote Sensing* (2023) [2](#), [4](#), [5](#), [9](#), [10](#), [11](#), [13](#)
70. Zagoruyko, S., Komodakis, N.: Learning to compare image patches via convolutional neural networks. In: CVPR. pp. 4353–4361 (2015) [4](#)
71. Zhang, H., Wu, C., Zhang, Z., Zhu, Y., Lin, H., Zhang, Z., Sun, Y., He, T., Mueller, J., Manmatha, R., et al.: Resnest: Split-attention networks. In: CVPR. pp. 2736–2746 (2022) [4](#)
72. Zhang, X., Yu, F.X., Kumar, S., Chang, S.F.: Learning spread-out local feature descriptors. In: ICCV. pp. 4595–4603 (2017) [4](#)
73. Zhao, T., Wu, X.: Pyramid feature attention network for saliency detection. In: CVPR. pp. 3085–3094 (2019) [4](#)
74. Zheng, W., Chen, Z., Lu, J., Zhou, J.: Hardness-aware deep metric learning. In: CVPR. pp. 72–81 (2019) [4](#)

Relational Representation Learning Network for Cross-Spectral Image Patch Matching (Supplementary Materials)

Chuang Yu^{1,2}, Yunpeng Liu^{1*}, Jinmiao Zhao^{1,2}, Dou Quan³, and Zelin Shi¹

¹ Shenyang Institute of Automation, Chinese Academy of Sciences

² University of Chinese Academy of Sciences

³ Xidian University

{yuchuang,ypliu,zhaojinmiao,zlshi}@sia.cn, dquan@stu.xidian.edu.cn

1 Feature Interaction Learning (FIL) Module

The feature interaction learning (FIL) module [8] can strengthen the interaction between cross-spectral image patch features and extract deeper feature relations, thereby ensuring the discriminability of the extracted features. From Fig. S-1, firstly, it uses a cross-attention mechanism to obtain the common features in one source that are the same as another source. Secondly, feature difference learning is performed on one source feature and the common feature that is the same as another source to extract private features. Generally, matching samples have many common features and few private features. For non-matching samples, the opposite is true. Meanwhile, both common features and private features extract features with the same attributes, such as edges, textures. It is unreasonable to directly fuse them to measure similarity. Therefore, to facilitate the generation of more discriminative private features, a metric network (module loss) is added to constrain the common features. In RRL-Net, we use the FIL module (five in total) for the corresponding cross-spectral feature maps generated at each stage.

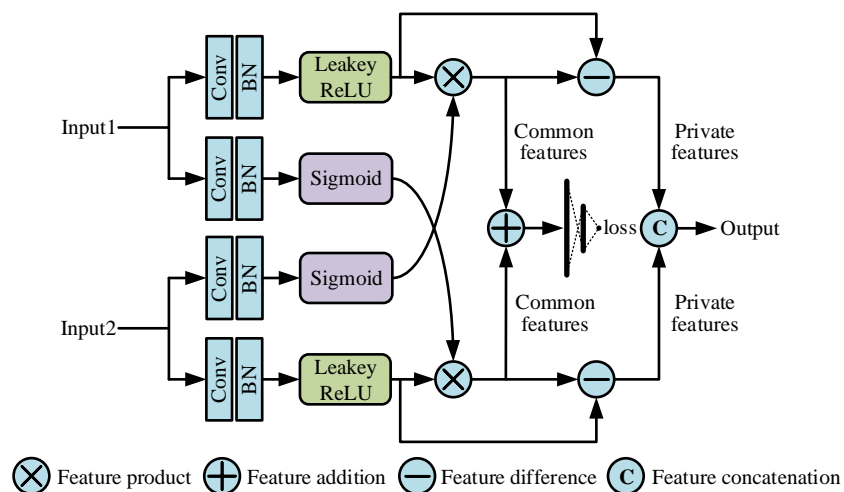


Fig. S-1: Feature interaction learning module.

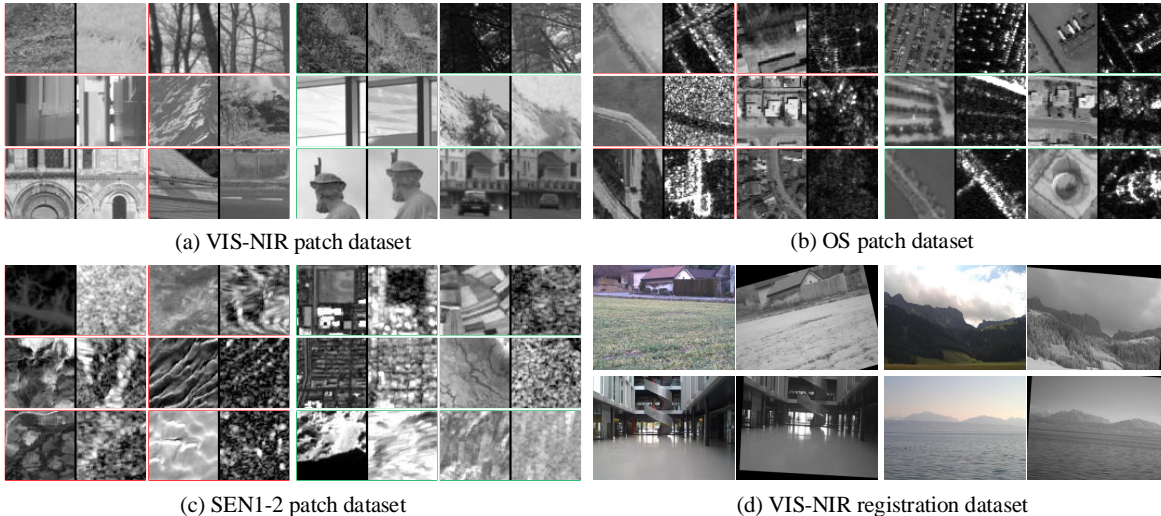


Fig. S-2: Partial sample display of multiple datasets. Red denotes non-matching samples. Green denotes matching samples.

For the output five-stage private features, we use feature aggregation operations to aggregate them sequentially to learn multi-scale discriminative features. For the metric network in the FIL module, it will be pruned before network model is saved to reduce parameters and improve the inference speed.

2 Detailed Introduction of the Datasets

From Fig. S-2, we experiment on four different cross-spectral datasets, in which the cross-spectral image patch size is 64×64 pixels. The details are as follows:

VIS-NIR patch dataset [1, 2]. It is a visible spectrum (VIS) and near-infrared (NIR) image patch matching dataset based on the VIS-NIR scene dataset [2]. Specifically, the dataset contains more than 1.6 million pairs of cross-spectral image patches with equal positive and negative samples, divided into 9 subsets. The detailed subset names and corresponding quantities are shown in Tab. S-1. For the construction of this dataset, VIS image patches cropped based on SIFT keypoints as the center are first acquired. Secondly, half of the VIS image patches and NIR image patches whose keypoint coordinates are consistent form matching samples. Finally, the other half of the VIS image patches and random NIR image patches form non-matching samples. In the experiment, the “Country” subset is used for training, and the remaining eight subsets are used for testing.

OS patch dataset [7, 9]. It is a VIS and SAR image patch matching dataset based on the OS dataset [7]. Each image patch is cropped at the center of the keypoints obtained by the SIFT method. Pairs of cross-spectral image patches with the same keypoints are identified as matching samples. Pairs of cross-spectral image patches with different keypoints are identified as non-matching samples. The number of generated non-matching samples is the same as the number of matching samples. The dataset contains a total of 123,676 samples, of which the training set and the test set contain 98,940 and 24,736 samples, respectively.

Table S-1: Number of image patch pairs for each subset in the VIS-NIR patch dataset.

Subset	Number	Subset	Number	Subset	Number
Country	277,504	Field	240,896	Forest	376,832
Indoor	60,672	Mountain	151,296	Oldbuilding	101,376
Street	164,608	Urban	147,712	Water	143,104

From Fig. S-2, compared with the VIS-NIR patch dataset, the VIS-SAR image patch pairs in the OS patch dataset have more obvious nonlinear differences.

SEN1-2 patch dataset [6, 8]. It is a VIS and SAR image patch matching dataset based on the SEN1-2 dataset [6]. The construction process of this dataset is consistent with that of the OS patch dataset. This dataset has more samples, containing a total of 800,000 samples, of which the training set and the test set contain 600,000 and 200,000 samples, respectively. From Fig. S-2, compared with the OS patch dataset, the scenes in the SEN1-2 patch dataset have less semantic feature information.

VIS-NIR registration dataset. This registration dataset is a VIS and NIR registration dataset that we construct based on the VIS-NIR scene dataset [2]. The image pair to be registered is generated by performing an affine transformation, including rotation, translation and scaling, on the NIR images in the original registered image pair. Consistent with the experiments on the VIS-NIR patch dataset, the experiments are trained on the “Country” subset and tested on the other eight subsets.

3 Detailed introduction of the evaluation metrics

3.1 Cross-spectral image patch matching task

For the cross-spectral image patch matching tasks, the false positive rate at 95% recall (FPR95) is used. The recall can also be called the true positive rate (TPR). FPR95 is the FPR corresponding to the TPR of 0.95 based on the ROC curve. The smaller the FPR95 is, the better the matching performance. The calculation formulas for the TPR (Recall) and FPR are as follows:

$$TPR = Recall = \frac{TP}{TP + FN} \quad (1)$$

$$FPR = \frac{FP}{FP + TN} \quad (2)$$

where TP denotes the number of results that predict positive samples as positive, TN denotes the number of results that predict negative samples as negative, FP denotes the number of results that predict negative samples as positive, and FN denotes the number of results that predict positive samples as negative.

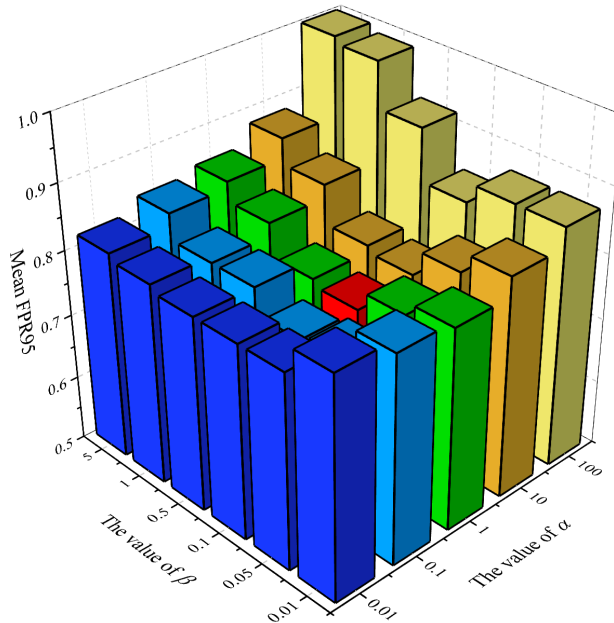


Fig. S-3: Experiment on the values of α and β . Red denotes the lowest value of 0.76.

3.2 Cross-spectral image registration task

For the Cross-spectral image registration task, the root mean square error ($RMSE$) and the image registration rate I_{rr} are used [4, 5, 8]. The smaller the $RMSE$ is, the better the registration effect. The larger the I_{rr} is, the better the registration effect.

$RMSE$ reflects the deviation between the registered image and the reference image. Its formula is as follows:

$$RMSE = \sqrt{\frac{1}{M} \sum_{i=1}^M [(rx_i)^2 + (ry_i)^2]} \quad (3)$$

where M denotes the number of matching point pairs and (rx_i, ry_i) denotes the error of the i_{th} matching point pair based on the transformation matrix.

I_{rr} reflects the overall performance of image registration. It denotes the ratio of the number of registered images to the total number of samples, and the formula is as follows:

$$I_{mp} = \frac{N_m}{N_{all}} \quad (4)$$

where N_m denotes the number of images whose $RMSE$ of the registered image is less than 5. N_{all} denotes the total number of test samples, which is 160 in the experiment.

4 Experiment on the values of α and β

We conducted experiments to explore the values of α and β , and the experimental results are shown in Fig. S-3. First, when the value of α is within 0.1-10 and the

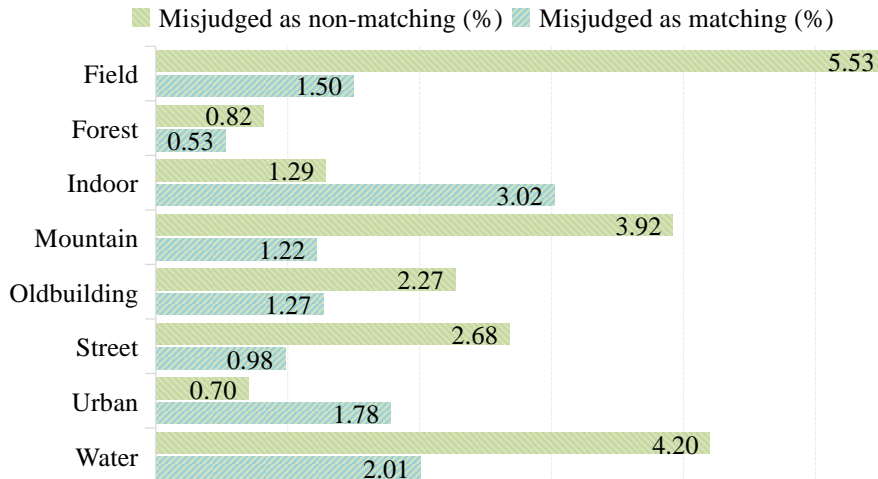


Fig. S-4: The misjudgment percentages of RRL-Net on eight subsets of the VIS-NIR patch dataset.



Fig. S-5: Some samples in the “Indoor” subset that are misjudged as matching.

value of β is within 0.05-0.5, RRL-Net has good matching results. This shows that RRL-Net has a certain degree of stability. At the same time, when α is 1 and β is 0.1, the network has the optimal matching result. In addition, when α is less than 1 or β is less than 0.1 and they become smaller and smaller, FPR95 shows an upward trend. This is because the constraint of the reconstruction branch will be weakened, resulting in insufficient intrinsic feature mining. When α is greater than 1 or β is greater than 0.1 and they become larger and larger, FPR95 also shows an upward trend and the trend is more obvious. The reason is that overemphasis on intrinsic feature mining and gradual neglect of subsequent feature relation mining will lead to insufficient discriminative feature extraction, resulting in a significant decrease in the matching effect.

5 Analysis of misjudgment percentage

To further quantitatively analyse the misjudgment of matching samples and non-matching samples by RRL-Net on the VIS-NIR patch dataset, we present the

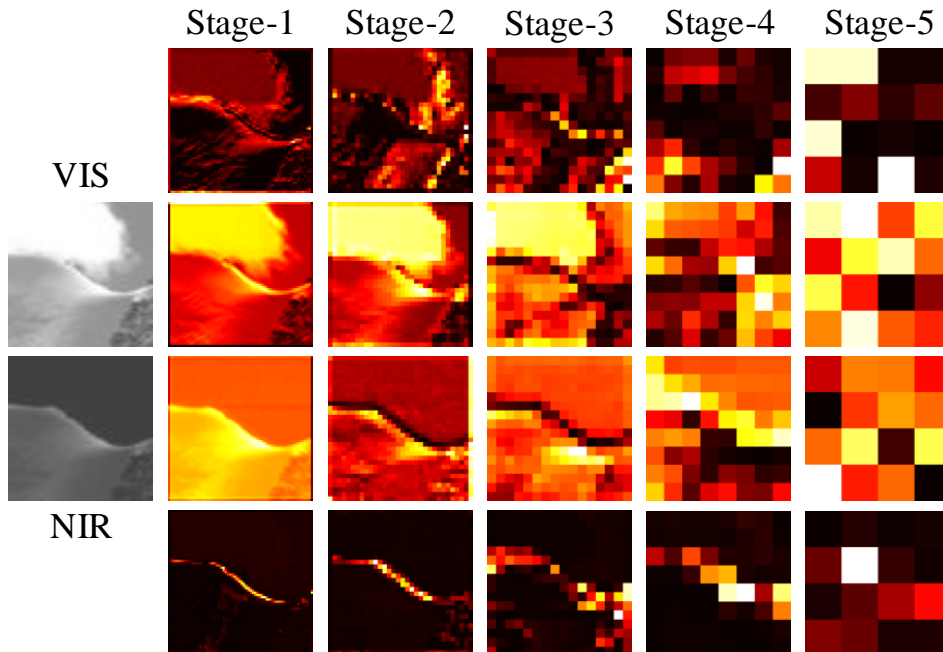


Fig. S-6: Visualization of the feature maps output by the MGLA modules and FIL modules for matching VIS-NIR samples. The middle two lines denotes the output of the MGLA module at each stage. The upper and lower lines denotes the private feature maps output by the FIL module at each stage.

misjudgment percentage of eight subsets, as shown in Fig. S-4. On the whole, the percentage of misjudged as non-matching is significantly greater than the percentage of misjudged as matching on the VIS-NIR patch dataset. On the one hand, this is because the experiment is trained on “Country” and tested on the other eight subsets. Therefore, the matching network can only approximately learn the domain information in the VIS-NIR image patch matching scenario. However, there are still scene differences in different subsets and non-linear differences between cross-spectral image patches. On the other hand, it is due to the spatiotemporal difference of collected images. Some moving objects or positional deviations of the shooting points will cause the samples that are finally marked as matching to appear visually non-matching. From the results of each subset, the percentage of samples in “Field”, “Mountain” and “Water” that are misjudged as non-matching is significantly larger. On the one hand, this is due to the influence of the environment. For example, wind has serious spatiotemporal effects on the targets (grass, clouds, and water waves) in the corresponding scene. On the other hand, this is due to the influence of the imaging conditions. The scenes in the three subsets are more likely to be too bright or too dark, resulting in a scarcity of single image features in the image patch pairs. This will lead to significant nonlinear differences between image patches. In addition, the “Indoor” subset has the highest percentage of misclassifications as matching. This is due to the large number of similar striped scenes in the scene. According to Fig. S-5, there are a large number of similar semantic features between such image patches, resulting in misjudgments as matching.

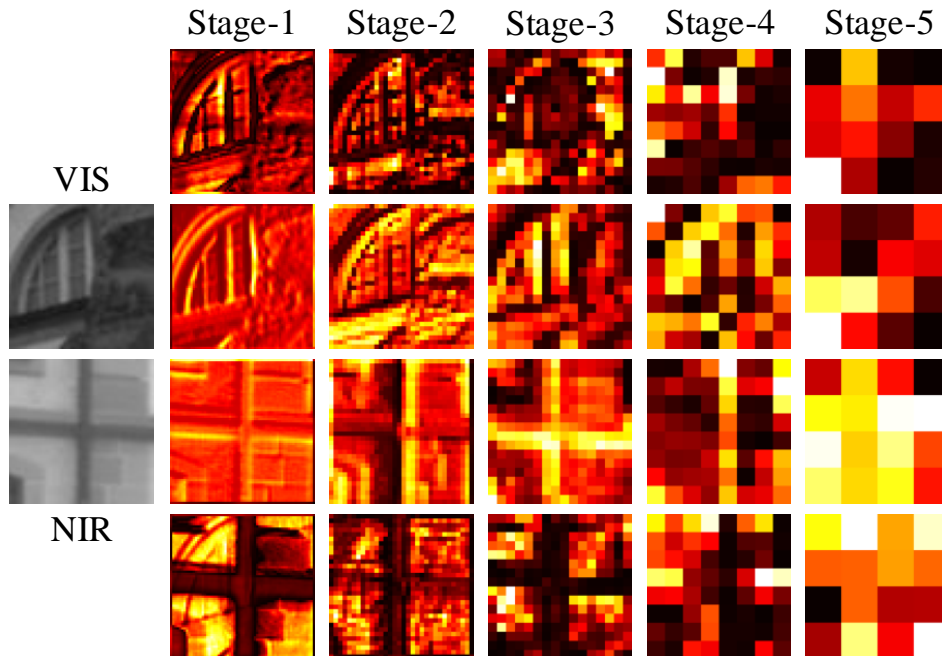


Fig. S-7: Visualization of the feature maps output by the MGLA modules and FIL modules for non-matching VIS-NIR samples. The middle two lines denotes the output of the MGLA module at each stage. The upper and lower lines denotes the private feature maps output by the FIL module at each stage.

6 Visualization of middle layer feature maps

To further qualitatively analyse the performance of the MGLA module (ALFE Network) and FIL module in RRL-Net, we visualize the feature maps output by the corresponding modules for matching samples and non-matching samples, as shown in Fig. S-6 and Fig. S-7. On the one hand, regardless of matching samples or non-matching samples, the feature map output by the MGLA module can well characterize the image features, and the overall brightness is relatively high. This shows that the ALFE network built based on the MGLA module can effectively fully characterize the intrinsic features of image patches. On the other hand, the private feature maps of matching samples are significantly darker than the feature maps output by the MGLA module and the private feature maps of non-matching samples. This verifies that the FIL module can effectively mine the deep-level relations between image patch features, thereby better measuring the similarity between image patches.

7 Visualization of cross-spectral image registration

To further verify the robustness and generalizability of RRL-Net, we applied RRL-Net to the cross-spectral image registration task. Fig. S-8 shows the partial registration results of RRL-Net on the eight test subsets on the VIS-NIR registration dataset. We can find that RRL-Net can generate a large number of matching points, and most of the predicted matching point pairs are correct

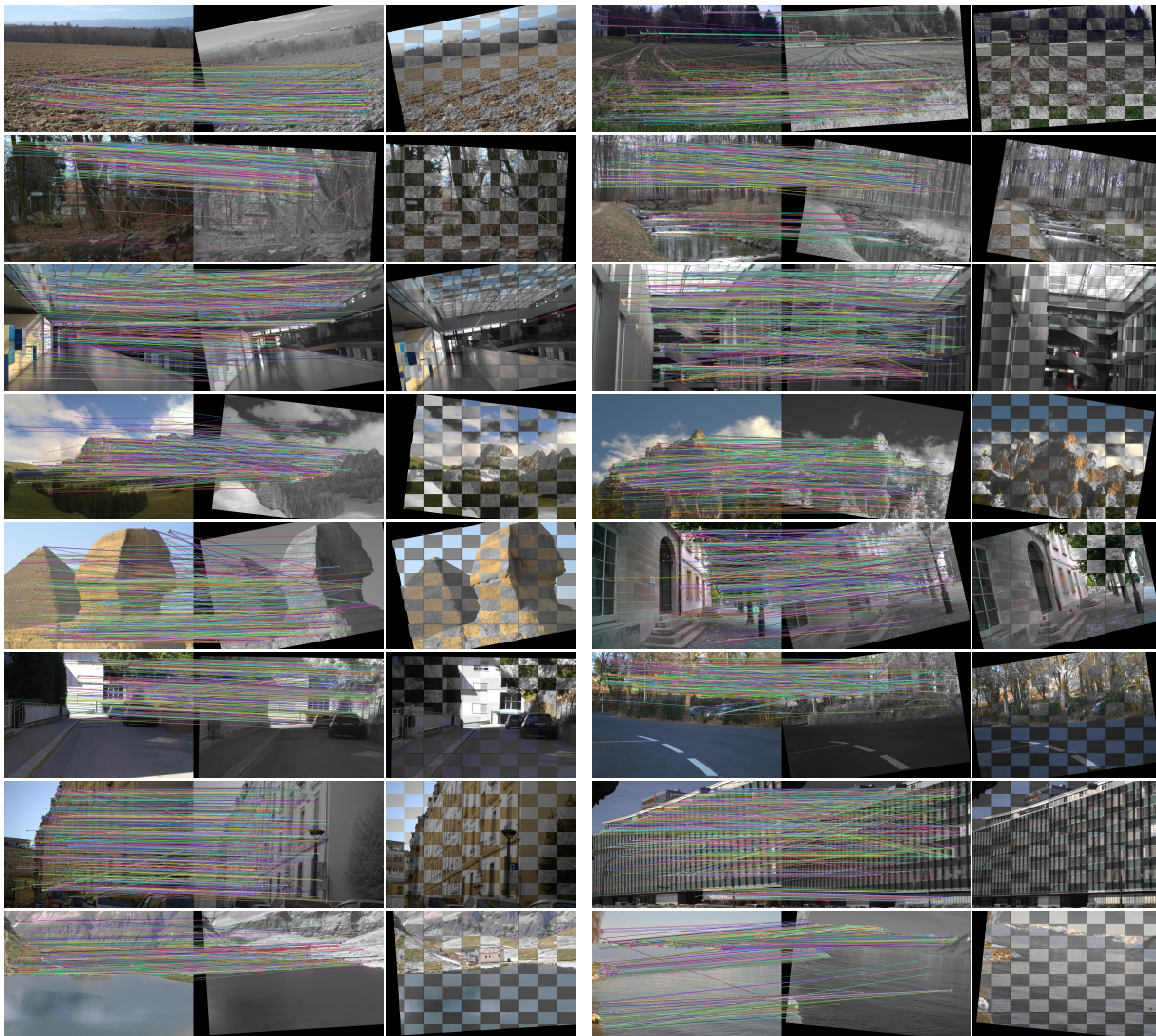


Fig. S-8: Partial registration results of RRL-Net on the VIS-NIR registration dataset. From top to bottom, the eight rows of samples come from the “Field”, “Forest”, “Indoor”, “Mountain”, “Oldbuilding”, “Street”, “Urban”, and “Water” subsets.

matching point pairs. For wrong matching point pairs, we use RANSAC [3] to remove and obtain the final affine transformation parameters. From the registered checkerboard image in Fig. S-8, it can be found that the VIS images after affine transformation almost completely overlap with the NIR images, which proves that RRL-Net has excellent registration results when applied to cross-spectral image registration.

References

1. Aguilera, C.A., Aguilera, F.J., Sappa, A.D., Aguilera, C., Toledo, R.: Learning cross-spectral similarity measures with deep convolutional neural networks. In: CVPRW. pp. 1–9 (2016) 2
2. Brown, M., Süssstrunk, S.: Multi-spectral sift for scene category recognition. In: CVPR. pp. 177–184 (2011) 2, 3

3. Fischler, M.A., Bolles, R.C.: Random sample consensus: a paradigm for model fitting with applications to image analysis and automated cartography. *Communications of the ACM* **24**(6), 381–395 (1981) [8](#)
4. Quan, D., Wang, S., Gu, Y., Lei, R., Yang, B., Wei, S., Hou, B., Jiao, L.: Deep feature correlation learning for multi-modal remote sensing image registration. *IEEE Transactions on Geoscience and Remote Sensing* **60**, 1–16 (2022) [4](#)
5. Quan, D., Wei, H., Wang, S., Lei, R., Duan, B., Li, Y., Hou, B., Jiao, L.: Self-distillation feature learning network for optical and sar image registration. *IEEE Transactions on Geoscience and Remote Sensing* **60**, 1–18 (2022) [4](#)
6. Schmitt, M., Hughes, L.H., Qiu, C., Zhu, X.X.: Sen12ms—a curated dataset of geo-referenced multi-spectral sentinel-1/2 imagery for deep learning and data fusion. *arXiv preprint arXiv:1906.07789* (2019) [3](#)
7. Xiang, Y., Tao, R., Wang, F., You, H., Han, B.: Automatic registration of optical and sar images via improved phase congruency model. *IEEE Journal of Selected Topics in Applied Earth Observations and Remote Sensing* **13**, 5847–5861 (2020) [2](#)
8. Yu, C., Liu, Y., Zhao, J., Wu, S., Hu, Z.: Feature interaction learning network for cross-spectral image patch matching. *IEEE Transactions on Image Processing* (2023) [1](#), [3](#), [4](#)
9. Yu, C., Zhao, J., Liu, Y., Wu, S., Li, C.: Efficient feature relation learning network for cross-spectral image patch matching. *IEEE Transactions on Geoscience and Remote Sensing* (2023) [2](#)